Analysis and Comparison of Two Wireless Battery Charger Arrangements for Electric Vehicles

Giuseppe Buja[1]*, *Rupesh K. Jha*[1], *Manuele Bertoluzzo*[1], *and Mude K. Naik*[2]
(1. Department of Industrial Engineering, University of Padova, Padova, Italy
2. Department of Electrical Engineering, AVVP University, Bengaluru, India)

Abstract: The paper deals with wireless battery chargers (WBCs) for plug-in electric vehicles (PEVs) and analyzes two arrangements for the receiver of a series-series resonant WBC. The first arrangement charges the PEV battery in a straightforward manner through a diode rectifier. The second arrangement charges the PEV battery through the cascade of a diode rectifier and a chopper whose input voltage is kept constant. Figures of merit of WBCs such as efficiency and sizing factor of both the power source and the transmitter/receiver coils are determined. Afterwards, they are discussed and compared with reference to the case study of WBC for an electric city car. A proposal to optimize the efficiency of the second arrangement by a suitable selection of the chopper input voltage is presented. Measurements on the efficiency of the two arrangements are included to support the theoretical results.

Keywords: EV battery charging, wireless charging, charging arrangement.

1 Introduction

Growing concern in greenhouse gas emissions from conventional gas and diesel powered vehicles has resulted in increased adoption of electric vehicles or plug-in hybrid electric vehicles, collectively termed plug-in electric vehicles (PEVs)[1]. Conventional wired charging of PEVs is not safe due to potential of the exposed conductors, interlocks, and connectors which may present electric shock hazards to users. Wireless battery chargers (WBCs) remove these risks, thus supporting growth of adoption of PEVs[2-3]. Today's WBCs exploit the inductive coupling[4] between a transmitting coil placed below the road surface and a receiving coil placed aboard PEV, and improve the power transfer capabilities of the inductive coupling by making the coils resonant with capacitors[5-7]. The capacitors are connected either in series or in parallel to the coils. Therefore, four topologies can be set up: series-series (SS), series-parallel, parallel-series and parallel-parallel[8-10]. From a comparative evaluation of the topologies based on the following figures of merit (FOMs): efficiency and sizing factor of the power source and the receiving coil, WBC with SS topology has been found to be most favorable and is here considered.

A schematic of resonant WBC is drawn in Fig.1. It is made of two stages, transmitter and receiver, with the transmitter that is fed by the grid and the receiver that charges the PEV battery. In addition to the resonant coil, each stage includes a power conversion circuit. That of the transmitter consists of a grid rectifier and a high-frequency voltage inverter with adjustable output. Due to the filtering action of the resonant transmitting coil, the power conversion circuitry behaves as a power source with sinusoidal voltage. The power conversion circuitry of the receiver includes a diode rectifier to supply the load with a direct voltage and resorts to different solutions for the adjustment of the voltage amplitude: in [11] the series resonant coil is connected to a switch that controls the magnitude of the AC voltage before applying it to the diode rectifier; in [12] this approach is extended to a parallel resonant coil; in [13] the loading capability of the circuitries in [11] and [12] is improved by an additional resonant section; in [14] the diode rectifier is substituted for by a controlled rectifier. The most popular solutions for a WBC receiver charge the battery either in a straightforward manner through a diode rectifier or through a chopper in cascade to the diode rectifier, and controls the voltage of the power source in the transmitter to adjust the power absorbed by the battery[15]. Two methods of charging the battery give rise to two WBC arrangements, hereafter denoted with #1 and #2 respectively.

The aim of this paper is to analyze and compare the two arrangements in terms of FOMs. Organization of the paper is as follows: Section 2 reviews basics on battery charging and introduces two additional FOMs,

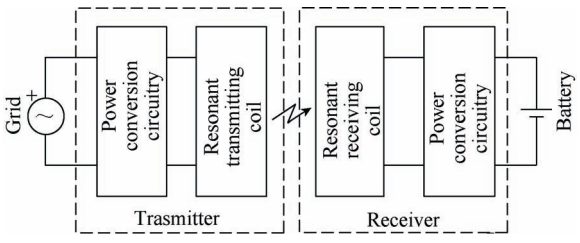

Fig.1 Resonant WBC schematic

* Corresponding Author, E-mail: giuseppe.buja@unipd.it.

namely power transfer ratio and receiver efficiency which are useful to evaluate the WBC efficiency. Section 3 determines the FOM expressions for a general SS resonant WBC topology. Section 4 analyzes the operation of the two arrangements. Section 5 discusses and compares the FOMs for the two arrangements with reference to the case study of an electric city car. Section 6 refers to arrangement #2 and investigates how FOMs change with the amplitude of the chopper input voltage. Section 7 reports on the measurements of efficiency for the two arrangements. Section 8 concludes the paper. An Appendix works out the relationship between the sizing factors of the receiving and transmitting coils.

Throughout the paper, sinusoidal quantities are represented by a phasor, denoted with a bar over the upper-case symbols, while their rms magnitudes are represented by upper-case symbols.

2 WBC background

2.1 Battery charging

A PEV battery is charged along two sequential modes: constant current (CC) and constant voltage (CV), as drawn in Fig.2. In the figure, V_B, I_B, P_B and R_B are the battery voltage, current, power absorbed by the battery, and the equivalent battery resistance, with the latter being defined as V_B/I_B; moreover, V_{co}, I_{co} and N are the cutoff voltage, the cutoff current and the point of transition from CC to CV mode. As a simplification, a linear profile is assumed for the battery voltage in CC mode. Voltage, current, power and resistance in Fig.2 are normalized respectively to V_M, I_{CC}, P_N, and R_N, where V_M is the maximum battery voltage, I_{CC} is the charging current in CC mode, P_N is the nominal charging power, given by the product of V_M by I_{CC} and reached at point N, and R_N is the equivalent battery resistance at point N, given by V_M/I_{CC}. The curves of Fig.2 show that, in addition to voltage and current, both resistance R_B and power P_B absorbed by the battery vary during charging. In particular, resistance R_B increases in CC mode from the initial value R_{Vco}, given by V_{co}/I_{CC}, to R_N at the CC mode completion, and continues to increase in CV mode up to R_{Ico}, given by V_M/I_{co}. In correspondence, the power absorbed by the battery increases from P_{Vco} to P_N and then decreases to P_{Ico}.

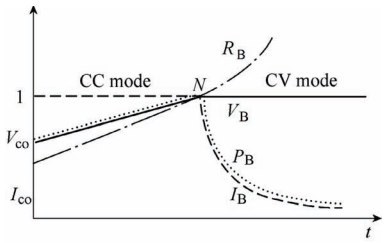

Fig.2 Battery charging: normalized profiles of voltage (solid line), current (dashed line), power (dotted line) and equivalent resistance (dashed-dotted line)

As a function of P_B, resistance R_B is expressed in CC and CV modes respectively as

$$R_B = I_{CC}^2 P_B \,, \quad R_B = V_M^2 \frac{1}{P_B} \tag{1}$$

2.2 WBC FOMs

Circuit diagram of SS resonant WBC is drawn in Fig.3. On the WBC transmitter side, $\bar{V}_S$, $\bar{I}_T$, C_T, $\bar{V}_{Tt}$, L_T, r_T and $\bar{V}_T$ are respectively the voltage of the power source, the transmitter current, the transmitting coil resonant capacitor, the voltage at the transmitting coil terminals, the transmitting coil inductance, the transmitting coil parasitic resistance, and the voltage induced in the transmitting coil. The magnitude of $\bar{V}_S$ is suitably adjusted along the battery charging process. On the WBC receiver side, $\bar{V}_R$, $\bar{I}_R$, L_R, r_R, $\bar{V}_{Rt}$, C_R, R_L, and $\bar{V}_L$ are respectively the voltage induced in the receiving coil, the receiver current, the receiving coil inductance, the receiving coil parasitic resistance, the voltage at the receiving coil terminals, the receiving coil resonant capacitor, the load resistance, representative of the equivalent battery resistance transferred to the receiver terminals, and the voltage across R_L.

The induced voltages are given by

$$\begin{cases} \bar{V}_T = j\omega M \bar{I}_R \\ \bar{V}_R = -j\omega M \bar{I}_T \end{cases} \tag{2}$$

where M is the mutual inductance between the coils and ω is the power source angular frequency.

Five FOMs are defined for WBC, namely overall efficiency (or simply, efficiency) η, power transfer ratio (PTR), receiver efficiency (RE), power source sizing factor (PSSF) and receiver coil sizing factor (RCSF). They are defined as

$$\eta \triangleq \frac{P_B}{P_S} \tag{3}$$

$$\text{PTR} \triangleq \frac{P_R}{P_S} \tag{4}$$

$$\text{RE} \triangleq \frac{P_B}{P_R} \tag{5}$$

$$\text{PSSF} \triangleq \frac{A_S}{P_N} \tag{6}$$

$$\text{RCSF} \triangleq \frac{A_R}{P_N} \tag{7}$$

where P_S, P_R, A_S and A_R are respectively the active power delivered by the power source, the active power transferred to the receiver, the sizing power of the power source and the sizing power of the receiving coil. As it can be readily seen, PTR represents the transmitter efficiency and the product of PTR by RE

gives the efficiency.

From the circuit diagram of Fig.3, the two sizing powers are expressed as

$$A_S = \max(V_S)\max(I_T) \tag{8}$$

$$A_R = \max(V_{Rt})\max(I_R) \tag{9}$$

where *max* stays for the maximum of the specified quantity along the battery charging process. Sizing power of the transmitting coil is correlated to that of the receiving coil, as documented in Appendix. PSSF and RCSF are an index of both cost and volume of WBC.

3 FOM expressions

FOMs are calculated for the circuit diagram of Fig.3, where the current in the load resistance R_L is equal to that of the receiver. By neglecting the losses of the circuitry between the receiver and the battery, the power entering into the load resistance coincides with the power P_B absorbed by the battery.

Let us examine the circuit of Fig.3 in resonance conditions. The impedance seen by $\overline{V}_R$ as well as by $\overline{V}_S$ is resistive. Then, currents $\overline{I}_R$ and $\overline{I}_T$ are in phase with the respective voltages $\overline{V}_R$ and $\overline{V}_S$, and the voltage equations for the two meshes are

$$V_S = r_T I_T + \omega M I_R \tag{10}$$

$$V_R = r_R I_R + V_L \tag{11}$$

Moreover, the relationship between the two currents, as calculated on the receiver side by help of (2), is

$$I_T = I_R \frac{r_R + R_L}{\omega M} \tag{12}$$

Efficiency, PTR and RE for the circuit diagram of Fig.3 can be written as

$$\eta = \frac{P_B}{P_{jT} + P_{jR} + P_B} \tag{13}$$

$$\mathrm{PTR} = \frac{P_{jR} + P_B}{P_{jT} + P_{jR} + P_B} \tag{14}$$

$$\mathrm{RE} = \frac{P_B}{P_{jR} + P_B} \tag{15}$$

where $P_{jT} = r_T I_T^2$ and $P_{jR} = r_R I_R^2$ are the power losses in the transmitter and receiver, respectively, and $P_B = R_L I_R^2$. By substituting these power expressions in (13)-(15) and by help of (12), one obtains

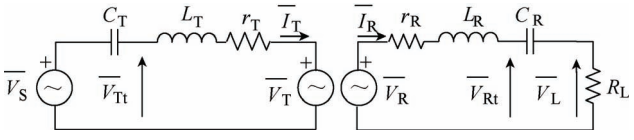

Fig.3 SS resonant WBC circuit diagram

$$\eta = \frac{R_L}{\frac{r_T}{(\omega M)^2} R_L^2 + \left[1 + \frac{2 r_T r_R}{(\omega M)^2}\right] R_L + r_R \left[1 + \frac{r_T r_R}{(\omega M)^2}\right]} \tag{16}$$

$$PTR = \frac{1}{\frac{r_T}{(\omega M)^2} R_L + \left[1 + \frac{r_T r_R}{(\omega M)^2}\right]} \tag{17}$$

$$RE = \frac{R_L}{r_R + R_L} \tag{18}$$

Equating to zero the derivative of (16) yields the value of R_L that gives the maximum efficiency

$$R_{L,\max} = \sqrt{\frac{r_R(\omega^2 M^2 + r_T r_R)}{r_T}} \tag{19}$$

By (16) and (19), the maximum efficiency is

$$\eta_{\max} = \frac{1}{\frac{2 r_T r_R}{(\omega M)^2} + \frac{2 r_T}{(\omega M)^2}\sqrt{\frac{r_R(\omega^2 M^2 + r_T r_R)}{r_T}}} \tag{20}$$

Eqs. (19) and (20) show that both $\eta_{\max}$ and $R_{L,\max}$ are dependent on the mutual inductance of the coils as well as on their parasitic resistances.

By (17) and (18), the maximum PTR is obtained for the minimum value of R_L while the maximum RE is obtained for the maximum value of R_L.

Calculation of the sizing factors of the power source and the receiving coil can be simplified by neglecting the parasitic resistances of the coils, without significantly impairing the results. Thus, by (10) and (12), V_S and I_T can be simplified as

$$V_S \cong \omega M I_R \tag{21}$$

$$I_T \cong \frac{R_L}{\omega M} I_R = \frac{V_L}{\omega M} \tag{22}$$

and PSSF is expressed as

$$\mathrm{PSSF} = \frac{\max(I_R)\max(V_L)}{P_N} \tag{23}$$

From the circuit diagram of Fig.3, the voltage across the receiving coil terminals is

$$\overline{V}_{Rt} = \overline{V}_R - \mathrm{j}\omega L_R \overline{I}_R \tag{24}$$

Since $\overline{I}_R$ is in phase $\overline{V}_R$, the two voltage terms on the right hand side of (24) are in quadrature, and V_{Rt} is equal to

$$V_{Rt} = \sqrt{(\omega M I_T)^2 + (\omega L_R I_R)^2} \tag{25}$$

By (2), eq. (25) becomes

$$V_{Rt} = \sqrt{V_R^2 + (\omega L_R I_R)^2} \tag{26}$$

and RCSF is expressed as

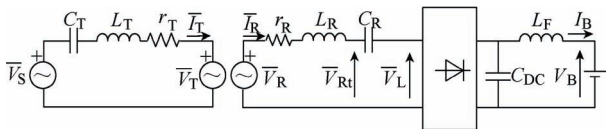

Fig.4 WBC arrangement #1 circuitry

$$\mathrm{RCSF}=\frac{\max\left[\sqrt{V_R^2+(\omega L_R I_R)^2}\right]\max(I_R)}{P_N} \tag{27}$$

4 WBC arrangement

4.1 Arrangement #1

Circuitry of arrangement #1 contains only a diode rectifier in the receiver. The circuitry is drawn in Fig.4, where capacitor C_{DC} and inductor L_F act as low-pass filters of the rectifier output voltage and current, respectively. Assuming ideal low-pass filtering, the voltage across capacitor C_{DC} is direct as well as the current through inductor L_F. According to the circuit operation, current $\bar{I}_R$ is rectified and its average value coincides with I_B. Moreover, the voltage across capacitor C_{DC} is equal to V_B and the voltage at the rectifier input is a square wave of magnitude V_B. Because of the filtering action of the resonant couple L_R-C_R, only the fundamental component $\bar{V}_L$ of the rectifier input voltage participates to the circuitry operation.

It is worthwhile to note that $\bar{V}_L$ is in phase with $\bar{I}_R$ so that the receiver sees a resistance at the input terminals of the rectifier. Such a resistance, previously termed as load resistance, is given by

$$R_L=\frac{V_L}{I_R} \tag{28}$$

where the rms values of $\bar{V}_L$ and $\bar{I}_R$, as a function of V_B and I_B, are

$$V_L=\frac{1}{\sqrt{2}}\frac{4}{\pi}V_B \tag{29}$$

$$I_R=\frac{1}{\sqrt{2}}\frac{\pi}{2}I_B \tag{30}$$

By (28)-(30), the load resistance is

$$R_L=\frac{8}{\pi^2}R_B \tag{31}$$

Eq. (31) shows that the load resistance is proportional to the battery resistance.

4.2 Arrangement #2

Circuitry of arrangement #2 contains a chopper in cascade to the diode rectifier in the receiver. The circuitry is drawn in Fig.5, where capacitor C_{DC} acts as a low-pass filter of the rectifier output voltage and inductor L_F as a low-pass filter of the chopper output current. As for arrangement #1, low-pass filtering is assumed ideal so that the chopper input voltage V_{DC} and the current through inductor L_F are direct. Current I_{DC} designates the direct component of the current upstream C_{DC}.

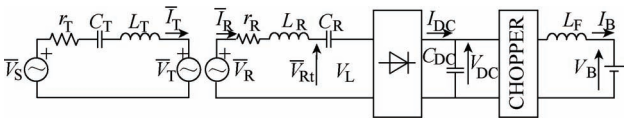

Fig.5 WBC arrangement #2 circuitry

Table 1 Battery and WBC data

Parameters	Symbol	Value
Battery voltages V_B/V	V_{co}, V_M	36, 56
Battery currents I_B/A	I_{CC}, I_{co}	10, 1
Battery resistances R_B/Ω	R_I, R_N, R_F	3.6, 5.6, 56
Battery power P_B/W	R_I, R_N, R_F	360, 560, 56
Trans. and rec. coil inductances/μH	L_T, L_R	120
Trans. and rec. coil parasitic resistance/Ω	r_T, r_R	0.5
Trans. and rec. resonant capacitances/nF	C_T, C_R	29
Mutual inductance/μH	M	30
Supply angular frequency/(rad/s)	ω	2π×85000

Operation of arrangement #2 differs from arrangement #1 as follows. Let V_{DC} be kept constant and not less than V_M in any charging condition. Then, the chopper adapts its input voltage V_{DC} to the battery voltage V_B with a duty-cycle δ equal to

$$\delta=\left(\frac{V_B}{V_{DC}}\right) \tag{32}$$

The duty-cycle along CC mode varies from V_{co}/V_{DC} to V_M/V_{DC} while in CV mode it remains constant at V_M/V_{DC}. Due to the duty-cycle, the resistance seen by capacitor C_{DC} is

$$R_{DC,B}=\frac{R_B}{\delta^2} \tag{33}$$

By substituting (32) in (33) and by replacing R_B in (31) with $R_{DC,B}$, the load resistance becomes

$$R_L=\frac{8V_{DC}^2}{\pi^2}\frac{R_B}{V_B^2} \tag{34}$$

Eq. (34) shows that the load resistance in CC mode is proportional to the battery resistance and inversely proportional to the square of the battery voltage, while in CV mode it is proportional to the load resistance only.

5 WBC arrangement analysis

5.1 Case Study

The case study in this paper is the prototype of SS resonant WBC for electric city-car presented in [16]. Battery and WBC data are listed in Table 1.

5.2 PTR, RE and efficiency

PTR, RE and efficiency along the battery charging process for the two arrangements are traced in Figs. 6-8 as a function of power P_B normalized to P_N. The curves ABC belong to arrangement #1 and those A'BC to arrangement #2. The curves in Figs. 6-8 are discussed in the subsequent Subsections for the battery charging process starting in CC mode at voltage V_{co}.

For arrangement #1, the load resistance in (16)-(18) is expressed in terms of P_B by means of (1) and (31) whereas, for arrangement #2, it is expressed in terms of P_B by means of (1) and (34). Analysis of arrangement #2 is carried out by setting V_{DC} at V_M. Then, according to (33), $R_{DC,B}$ decreases from 8.7 to 5.6 Ω (i.e. the value of R_N) in CC mode and coincides with R_B in CV mode. Note that, for arrangement #1, R_B increases from 3.6 to 5.6 Ω in CC mode.

5.3 Arrangement #1

PTR: at V_{co}, PTR is calculated as 0.992 and is indicated with point A in Fig.6. By (11) and (29), while the battery charging process goes on in CC mode, the voltage V_R increases linearly with V_B. By (2), this involves a proportional increase of I_T and a power-of-two increase of the power losses in r_T. In turn, the active power transferred to the receiver increases proportionally to V_B. In the aggregate, PTR decreases to 0.988 at the CC mode completion (point B). In CV mode, the voltage V_R is nearly constant and the same occurs for the power losses in r_T while power P_B decreases. Therefore, PTR decreases, moving from point B to C, where PTR gets the minimum value of 0.904. In the PTR curve as well in RE and efficiency curves, it should be noted that point A' along the CV mode curve has the same power P_B of point A.

RE: at V_{co}, RE is calculated as 0.83 and is indicated with point A in Fig.7. While the battery charging process goes on in CC mode, the power losses in r_R remain constant while power P_B increases. Correspondingly, RE increases to 0.88 at the CC mode completion (point B). In CV mode, the power losses in r_R decrease with the square of the current while power P_B decreases proportionally to the current. In the aggregate, RE increases up to 0.98 (point C).

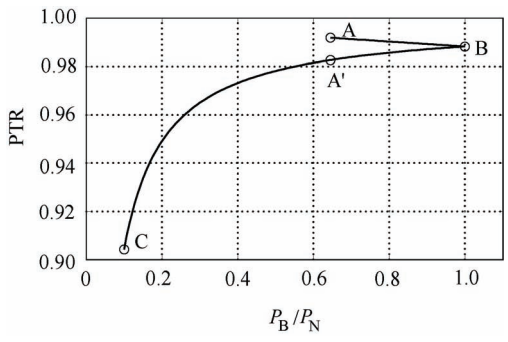

Fig.6 PTR for WBC arrangement #1 and #2

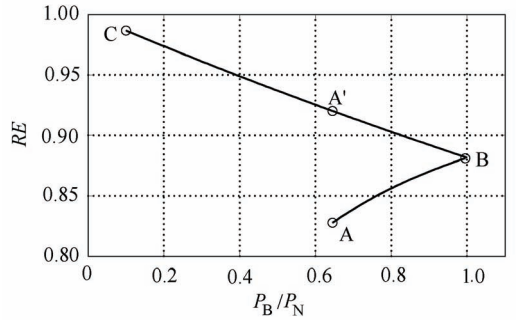

Fig.7 RE for WBC arrangements #1 and #2

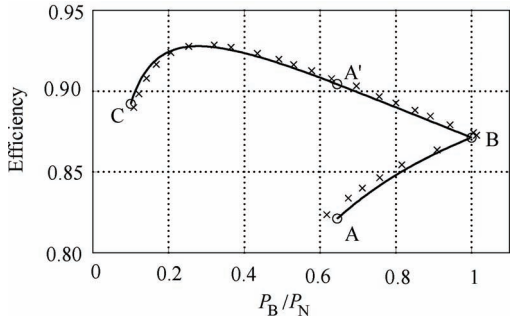

Fig.8 Efficiency for arrangements #1 and #2 and experimental results

Efficiency: at V_{co}, power P_B is 360W. The relevant efficiency is calculated to be 0.82 and is indicated with point A in Fig.8. While the battery charging process goes on in CC mode, the increase in RE prevails on the decreases of PTR. Indeed, the power losses in r_R are constant while those in r_T increase but remain lower. This because in CC mode it is $\omega M > R_L + r_R$ and hence, by (12), current I_T is less than current I_R. Correspondingly, the efficiency increases from point A to B, which is reached at the CC mode completion point and has coordinates of P_B=560W, h=0.87.

In CV mode there is an increase of RE concurrently with a decrease of PTR. Efficiency continues to increase until the power losses in r_R are greater than in r_T; afterwards, the decrease in PTR prevails on the increase of RE and the efficiency decreases. The efficiency curve is BA'C, with efficiencies of 0.9 and 0.89 at points A' and C, respectively. The curve exhibits a maximum of 0.93 for a value of P_B, denoted as $P_{B,max}$, equal to 156W. By (19), the corresponding value of $R_{L,max}$ is 16.3Ω that, according to the data in Table 1, is just a value taken by the load resistance within the CV mode.

5.4 Arrangement #2

The main feature of arrangement #2 is operation at constant chopper input voltage, which means that voltage V_L remains constant all along the charging process at the value given by (29), provided that V_B is substituted for by V_M. Therefore, the PTR, RE and efficiency curves differ from those of arrangement #1 only in CC mode.

Power P_B absorbed in CC mode by the battery is

equal to the power absorbed in the interval of CV mode extending from P_{co} (abscissa of point A' of the curves) to P_N (abscissa of point B of the curves), where P_{co} is the power value absorbed in CC mode at V_{co}. On the other hand, resistance $R_{DC,B}$ in CC mode mirrors R_B in the interval of CV mode. Therefore, the PTR, RE and efficiency curves in CC mode are given by that portion of the curves in CV mode departing from A' and arriving at B.

A short explanation of the curve profiles in CC mode is given below. Instrumental in the explanation is the following equation that equates the power absorbed by the battery to that absorbed by the chopper:

$$I_{DC} = \frac{I_{CC}}{V_M} V_B \tag{35}$$

By replacing I_B in (30) with I_{DC}, current I_R is obtained. Eq. (35) puts in evidence that here, differently from arrangement #1, it is current I_R and not voltage V_R that increases in CC mode on account of the increase of voltage V_B.

PTR: tat V_{co}, PTR is given by point A' in Fig.6. While the battery charging process goes on in CC mode, the power losses in r_T are nearly constant while the power transferred to the receiver increases. Then, PTR increases up to point B, which is reached at the CC mode completion.

RE: at V_{co}, RE is given by point A' in Fig.7. While the battery charging process goes on in CC mode, the power losses in r_R increase at the square of I_R while power P_B increases linearly with it. Then, PTR decreases to point B, which is reached at the CC mode completion.

Efficiency: at V_{co}, efficiency is given by point A' in Fig.8. While the battery charging process goes on in CC mode, the decrease in RE prevails on the increase of PTR because, by (12), the change of the power losses in r_R is much greater than in r_T. Then, the efficiency decreases to point B, which is reached at the CC mode completion.

5.5 Efficiency comparison

The curves of Fig.8 indicate that the efficiency in CC mode is higher for arrangement #2. This is because, along the CC mode, the following occurs: i) current I_R is lower than with arrangement #1; then, compared to arrangement #1, the power losses in r_R are lower, ii) voltage V_L stays constant at its maximum value, reached only at the CC mode completion for arrangement #1; then, compared to arrangement #1, the power losses in r_T are greater, and iii) current I_R is greater than I_T and the influence on the efficiency of the power losses in r_R overcomes that of the power losses in r_T.

5.6 PSSF and RCSF

By (23), calculation of PSSF needs to find the maximum of I_R and V_L. For both the arrangements, the maximum of I_R is $I_R = \frac{1}{\sqrt{2}} \frac{\pi}{2} I_{CC}$ and the maximum of V_L is $V_L = \frac{1}{\sqrt{2}} \frac{4}{\pi} V_M$. Therefore, PSSF is equal to 1. Accounting for parasitic resistances, the calculation of PSSF would result in 1.14, due to excess in voltage V_S to face with the voltage drops across the parasitic resistances.

By (27), calculation of RCSF needs to find the maximum of $\sqrt{(V_R)^2 + (\omega L_R I_R)^2}$ and I_R. For both arrangements, the maximum of $\sqrt{(V_R)^2 + (\omega L_R I_R)^2}$ is achieved at point N of the charging profile, where V_R and I_R get their maximum values concomitantly. Regarding the maximum of I_R, the same applies as for PSSF. By (34), RCSF results in 14.15. If the parasitic resistances are accounted for, the calculation of RCSF would result in 14.16, which is evidence of the fact that the parasitic resistances have little impact on RCSF.

By(25) and (2), V_R is somewhat less than $\omega L_R I_R$ since both the following inequalities apply: $M < L_R$ and $I_T < I_R$. Thus, RCSF can be approximated as

$$\text{RCSF} \cong \frac{\pi^2}{8} \frac{\omega L_R}{R_N} \tag{36}$$

Eq. (36) shows that RCSF is about equal to the quality factor of the receiving coil loaded with the equivalent battery resistance at point N of the charging profile.

6 Chopper input voltage selection

An issue can arise regarding the selection of the amplitude of the chopper input voltage V_{DC} for arrangement #2. To investigate this issue, efficiency has been calculated, for $V_{DC}=V_M$ as well as for two other values of V_{DC}, namely $1.2V_M$ and $1.4V_M$. The results are traced in Fig.9.

First of all, it emerges from Fig.9 that the efficiency curves retain the same profile as for $V_{DC}=V_M$. However, the efficiency increases with voltage V_{DC} for high values

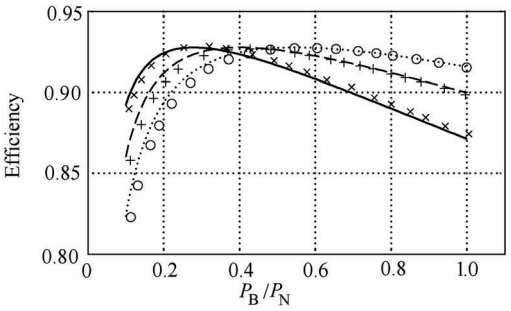

Fig.9 Efficiency for arrangement #2with $V_{DC}=V_M$ (blue solid line), $V_{DC}=1.2\ V_M$ (dashed red line) and $V_{DC}=1.4\ V_M$(green dotted line) and experimental results

of power P_B, while the opposite occurs for low values of power P_B. This behavior arises from the opposite effects of voltage V_{DC} on the power losses in r_R and r_T; actually, against an increase of voltage V_{DC}, the power losses in r_R decrease because of the lower values of I_R while those in r_T increase because of the higher values of I_T. Therefore, effect of the power losses in r_R predominates at higher values of power P_B, when I_R approaches its maximum value, while effect of the power losses in r_T predominates at the lower values of power P_B. Moreover, the efficiency curves exhibit i) an equal maximum, and ii) a shift of the abscissa $P_{B,max}$ of the maximum towards the higher values of power with the increase of voltage V_{DC}. Regarding the last point, $P_{B,max}$, calculated from (1) and (34) with voltage V_B set at V_M, is expressed as

$$P_{B,max} = \frac{8}{\pi^2}\frac{V_{DC}^2}{R_{L,max}} \tag{37}$$

showing that the abscissa of the maximum efficiency effectively increases with V_{DC} (at the square-of-two).

PSSFs calculated for the three values of V_{DC} by accounting for the parasitic resistances are: 1.14 for V_{DC}=V_M, 1.11 for V_{DC}=1.2V_M and 1.09 for V_{DC}=1.4V_M, underlining a small decrease of PSSF at higher values of V_{DC}. RCSFs, in turn, are 14.16, 9.86 and 7.28, underlining an appreciable decrease of RCSF at the higher values of V_{DC}. For both the factors, the reduction in their values is due to the reduction in I_R that, in turn, decreases the voltage drop across L_R.

The results of Fig.9 suggest that the most convenient selection for V_{DC} is to set $P_{B,max}$ in the middle of the interval of power P_B with extremes P_{co} and P_N. There are two reasons at the basis of this selection:

(1) Most of the charge of the battery is done in CC mode and in the successive interval of CV with equal values of power P_B.

(2) Most of the energy flows through WBC with power levels comprised between P_{co} and P_N. For the case study, such a value of $P_{B,max}$ is 460 W and it is obtained for V_{DC} equal to 1.7 V_M.

7 Experimental analysis

The theoretical results on the efficiency have been supported through experimental analysis executed on SS resonant WBC having the specifications reported in Table 1. Both arrangements have been implemented and a variable resistor has been used to emulate the battery. A first set of test has been carried out by adjusting the variable resistor so as to reproduce operation of arrangement #1. The efficiency of WBC and the power absorbed by the variable resistor have been measured by wattmeter WT1800 of Yokogawa. The measurements are reported with marks *x* in Fig.8; they are in nearly perfect agreement with the curve obtained from the theory.

Afterwards, operation of arrangement #2 has been reproduced by operating at constant V_{DC}; besides V_{DC}=V_M, the experiments have been repeated by setting V_{DC} at 1.2 V_M and 1.4 V_M. The measures of efficiency are reported with marks + for V_B=1.2 V_M and with marks o for V_B= 1.4 V_M in Fig.10. Marks *x* still refer to V_B=V_M. Also these measurements match well the theoretical results, confirming that the value of the maximum efficiency of WBC i) does not depend on V_{DC}, and ii) is reached at higher values of power absorbed by the battery as V_{DC} increases.

8 Conclusions

The paper has examined two different WBC arrangements for PEVs, one with the receiver that charges the battery through a diode rectifier and the other one through a chopper in cascade to the diode rectifier. Expression of FOMs (efficiency, power transfer ratio, receiver efficiency and sizing factor of both the power source and the receiving coil) of the two arrangements has been formulated as a function of the power absorbed by the battery, and calculated for the case study of SS resonant WBC for an electric city car. Comparison of the FOMs have shown the benefits of using the arrangement with the chopper. Afterwards, FOMs of this arrangement have been evaluated for different amplitudes of the chopper input voltage, revealing that a higher voltage is beneficial for all the FOMs, except for the efficiency when the transferred power is low. The theoretical results on efficiency have been supported by an experimental analysis.

Appendix

The sizing factor of the receiving coil is given by (9), where max(V_{Rt}) is the maximum of the voltage across the receiver coil terminals. Similarly, the sizing factor of the transmitting coil is expressed as

$$A_T = \max(V_{Tt})\max(I_T) \tag{A1}$$

where max(V_{Tt}) is the maximum of the voltage across the transmitting coil terminals. From the circuit diagram of Fig.3, it is

$$\bar{V}_{Tt} = \bar{V}_T + j\omega L_T \bar{I}_T \tag{A2}$$

Since $\bar{I}_T$ is in phase with $\bar{V}_T$, the magnitude of $\bar{V}_{Tt}$ is

$$V_{Tt} = \sqrt{(\omega M I_R)^2 + (\omega L_T I_T)^2} \tag{A3}$$

The maximum of V_{Tt} is achieved at point N of the charging profile, where both I_R and I_T get their maximum values. By (25), the relationship between A_T and A_R can be written as

$$A_T = \frac{\sqrt{(M)^2 + \left[L_T \dfrac{\max(I_T)}{\max(I_R)}\right]^2}}{\sqrt{(M)^2 + \left[L_R \dfrac{\max(I_R)}{\max(I_T)}\right]^2}} A_R \tag{A4}$$

For (22) calculated at point N, (A4) becomes

$$A_T = \frac{\sqrt{(M)^2 + \left(\frac{8L_T R_N}{\pi^2 \omega M}\right)^2}}{\sqrt{(M)^2 + \left(\frac{\pi^2 L_R \omega M}{8R_N}\right)^2}} A_R \qquad \text{(A5)}$$

underlining that the relationship between the sizing factors of the transmitting and receiving coils depends on the inductive parameters of the coils and the equivalent battery resistance at point N of the charging profile.

References

[1] D. P. Tuttle, and R. Baldick, "The evolution of plug-in electric vehicle grid interactions," *IEEE Transactions on Smart Grid*, vol. 3, no. 1, pp. 500-505, 2012.

[2] Y. Kaneko, and S. Abe, "Technology trends of wireless power transfer systems for electric vehicle and plug-in hybrid electric vehicle," Proc. *IEEE 10th Int. Conf. on Power Electronics and Drive Systems(PEDS)*, 2013, pp. 1009-1014.

[3] Li Siqi, and C.C. Mi, "Wireless power transfer for electric vehicle applications," *IEEE Journal of Emerging and Selected Topics in Power Electronics*, vol. 3, no. 1, pp. 4-17, 2015.

[4] X. C. Wei, E. P. Li, Y. L. Guan, and Y. H. Chong, "Simulation and experimental comparison of different coupling mechanisms for the wireless electricity transfer," *Journal of Electromagnetic Waves and Applica- tions*, vol. 27, no.7, 2009.

[5] G.A. Covic, and J. T. Boys, "Modern trends in inductive power transfer for transportation applications," *IEEE Journal of Emerging and Selected Topics in Power Electronics*, vol.1, no. 1, pp. 28-41, 2013.

[6] J. T. Boys, and G. A. Covic, "The inductive power transfer story at the university of auckland," *IEEE Circuits and Systems Magazine*, vol. 15, no. 2, pp.6-27, 2015.

[7] S.Y. Choi, B.W. Gu, S.Y. Jeong, and C.T. Rim, "Advances in wireless power transfer systems for roadway-powered electric vehicles," *IEEE Journal of Emerging and Selected Topics in Power Electronics*, vol.3, no.1, pp.18-36, 2015.

[8] W. Zhou, and H. Ma, "Design considerations of compensation topologies in ICPT system," *Proc. of. IEEE Conf. on Applied Power Electronics*, 2007, pp. 985-990.

[9] W. Li, C.C. Mi, S. Li, J. Deng, T. Kan, and H. Zhao, "Integrated LCC compensation topology for wireless charger in electric and plug-in electric vehicles," *IEEE Transactions on Industrial Electronics*, vol. 62, no. 7, pp. 4215-4225, 2014.

[10] C. Wang, O. H. Stielau, and G. A. Covic, "Design considerations for a contactless electric vehicle battery charger," *IEEE Transactionson Industrial Electronics*, vol. 52, no. 5, pp. 1308-1314, 2005.

[11] H. H. Wu, G.A. Covic, J. T. Boys, and D. J. Robertson, "A series-tuned inductive-power-transfer pickup with a controllable AC-voltage output," IEEE Transactions on Power Electronics, vol. 26, no. 1, pp. 98-109, 2011.

[12] H. H. Wu, J. T. Boys, and G. A. Covic, "An AC processing pickup for IPT systems," *IEEE Transactions on Power Electronics*, vol. 25, no. 5, pp. 1275-1284, 2010.

[13] J. E. James, D. J. Robertson, and G. A. Covic, "Improved AC pickups for IPT Systems," *IEEE Transactions on Power Electronics*, vol. 29, no. 12, pp. 6361-6374, 2014.

[14] L. J. Zou, A. P. Hu, D. Robertson, and B. Wang, "A new rectifier with combined power flow control capability for a series-tuned inductive-power-transfer receiver," *Proc. IEEE International Conference on Power System Technology (POWERCON)*, 2012, pp. 1-6.

[15] K. Colak, M. Bojarski, E. Asa, and D. Czarkowski, "A constant resistance analysis and control of cascaded buck and boost converter for wireless EV chargers," *Proc. IEEE* Applied Power Electronics Conference and Exposition (APEC), 2015, pp. 3157-3161.

[16] G. Buja, M. Bertoluzzo, and K. N. Mude, "Design and experimentation of WPT charger for electric city-car", *IEEE Transactions on Industrial Electronics*, vol. 62, no. 62, pp. 7436-7447, 2015.

Giuseppe Buja is a Full Professor of the University of Padova, Italy, heading the laboratory on "Electric Systems for Automation and Automotive". He has carried out research in the field of power and industrial electronics, especially of static converters, electric drives and DSP control systems. He has authored or co-authored more than 200 papers published in international journals and conferences. His current research is turned to wired and wireless charging of the electric vehicles, and to power conversion systems for renewable energies. He was the recipient of the IEEE Industrial Electronics Society Eugene Mittelmann Achievement Award "in recognition of his outstanding technical contributions to the field of industrial electronics".

Rupesh Kumar Jha received his B. Tech. degree in Electrical and Electronics Engineering from Biju Patnaik University of Technology, Rourkela (India) in 2012 and M. Tech. degree in Electrical Engineering with specialization Power Electronics from Birla Institute of Technology, Mesra (India) in 2014. His master thesis was on Fault Tolerance of Permanent Magnet Brushless DC Motor Drive Currently he is pursuing Ph. D. degree in Science, Technology and Mechanical Measurements for Engineering and Space, at the University of Padova, Italy, working in the Laboratory of Electric Systems for Automation and Automotive of the Department of Industrial Engineering. His current research is on power supply and control of wireless power transfer systems for electric vehicles.

Manuele Bertoluzzo received the M.S. degree in electronic engineering and the Ph.D. degree in industrial electronics and computer science from the University of Padova, Padova, Italy, in 1993 and 1997, respectively. From 1998 to 2000, he was a member of the Research and Development Division of an electric drive factory. In 2000, he joined the Department of Electrical Engineering, University of Padova, as a Researcher in the Scientific Disciplines' Group "electric converters, machines, and drives." Since 2015, he is Associate Professor and holds classes on Enertronics and Road Electric Vehicles. He is currently involved in the analysis and design of power electronics and control systems for electric and hybrid vehicles and for wireless power transfer systems.

Kishore Naik Mude received his B. Tech. degree in Electrical Engineering from Sri Venkateswara University, Tirupati, India, in 2008, his M.Tech. degree in Electrical Engineering from the Motilal Nehru National Institute of Technology, Allahabad, India, in 2010. From 2010 to 2011, he was a Lecturer at Amity University, Noida, India.From 2012 to 2014 he attended the Ph.D course in Electrical Engineering at University of Padova, Italy, receiving the Ph.D.degree in March 2015. Presently he is working with Amrita Vishwa Vidyapeetham University, Bengaluru campus, India. Recently he was invited for talks on wireless battery chargers in USA and Canada. His research interests are inductive power transfer systems for electric vehicles and battery chargers.